



Silicon substituted hydroxyapatite: Preparation with Solid-State Reaction, Characterization and Dissolution Properties

M. Jamil, B. Elouatli, H. Khallok, A. Elouahli, E. Gourri, M. Ezzahmouly, F. Abida, Z. Hatim

*Electrochemical and biomaterials team Chemistry Department,
Faculty of Sciences. Chouaib Doukkali University, BP 20, El Jadida, Morocco*

Received 08 Dec 2017,
Revised 11 Apr 2018,
Accepted 01 May 2018

Keywords

- ✓ Bioceramics,
- ✓ Hydroxyapatite,
- ✓ Silicon,
- ✓ Solid-state reaction,
- ✓ Dissolution.

mo.jamil@yahoo.fr

Abstract

Silicon substituted hydroxyapatite ($\text{Ca}_{10}(\text{PO}_4)_{5.5}(\text{SiO}_4)_{0.5}(\text{OH})_{1.5}$; Si-HAP) and unsubstituted hydroxyapatite ($\text{Ca}_{10}(\text{PO}_4)_6(\text{OH})_2$; HAP) are prepared by solid-solid reaction at 1100°C from intimate mixtures of tricalcium phosphate ($\beta\text{-Ca}_3(\text{PO}_4)_2$), calcium carbonate (CaCO_3) with or without silicon dioxide (SiO_2). The prepared ceramics were characterized by Fourier Transform Infrared spectroscopy (FTIR) and X-ray Diffraction (XRD). Their dissolution was carried out in a buffer solution ($\text{pH} = 4.8$) at 37°C . From the analysis of the XRD patterns, HAP and Si-HAP, have been identified as single phase. The results of FTIR and the structural refinement show and confirm the incorporation of the silicate ion in the HAP structure. The substitution of PO_4^{3-} by SiO_4^{4-} groups causes a reduction of the hydroxyl groups and increase the lattice distortion index ($D_{\text{ind}} = 4.682$) compared to the pure HAP value ($D_{\text{ind}} = 4.156$) and the theoretical HAP value ($D_{\text{ind}} = 3.079$). This structural change increases the dissolution of HAP which would lead to an improvement of its biological activity.

1. Introduction

Calcium hydroxyapatite ($\text{Ca}_{10}(\text{PO}_4)_6(\text{OH})_2$; HAP) is the principal mineral component of bone [1]. For this reason, it is known for its applications in medicine as synthetic bone substitutes [2]. Low solubility and bioactivity of HAP have classically limited its use in clinical applications [3,4]. In the bone, the hydroxyapatite presents different ionic substitutions, such as sodium, magnesium, carbonate or silicate [5, 6]. The special attribute of HAP structure lies in its ability to accept a large number of anionic and cationic substituents. To improve the solubility and the bioactivity of the hydroxyapatite, several researchers have incorporated different ionic substituents into synthetic HA to produce a mineral composition more akin to that of natural bone tissue [7,8].

The silicon (Si) has been identified as an important element in the bone [9, 10]. The inclusion of silicates in the apatite structure causes an acceleration of the dissolution and stimulates the action of osteoblasts and therefore plays a role in the calcification process [11-13]. It has been reported that in vitro Si enhances and stimulates osteoblast-like cell activity [14,15] and in vivo induces a higher dissolution rate [14,16]. Moreover, several studies suggest better biological activity of Si-substituted calcium phosphates with respect to unsubstituted calcium phosphates [14,17-19].

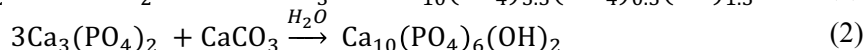
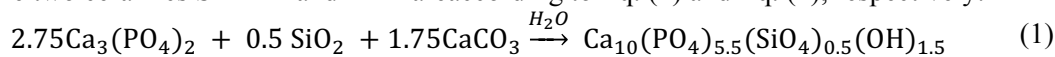
Several synthesis methods of silicon substituted hydroxyapatite have been proposed, such as the wet chemical preparation, the hydrothermal process and solid state reaction [20-25]. Wet precipitation and hydrothermal preparation became more popular methods, but conventional precipitation has a poorer ability to control the Ca/P ratio. The introduction of silicates in calcium-hydroxyapatite is possible by solid-solid reaction. However, the solid-state reaction requires high temperatures over 1300°C with repeated grinding and calcinations cycles to obtain a quasi stoichiometric product [25]. This method may, however, remain suitable in view of a large production of powder (i.e. industrial).

The objective of this study is the preparation, by a solid-state route, of monophasic powders of silicon substituted and unsubstituted hydroxyapatite with single calcination step at a relatively low temperature. We studied the incorporation effect of silicon on the structure and on the solubility of hydroxyapatite ceramics.

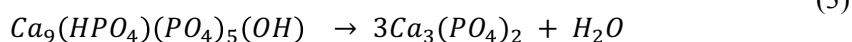
2. Material and Methods

2.1. Powders preparation

Si-HAP ($\text{Ca}_{10}(\text{PO}_4)_{5.5}(\text{SiO}_4)_{0.5}(\text{OH})_{1.5}$) ceramics was performed by solid-solid reaction from a mixture of β -tricalcium phosphate ($\beta\text{-Ca}_3(\text{PO}_4)_2$), silicon dioxide (SiO_2) and calcium carbonate (CaCO_3). Unsubstituted hydroxyapatite HAP ($\text{Ca}_{10}(\text{PO}_4)_6(\text{OH})_2$) has also been prepared. The chemical reactions involved in the preparation of the two ceramics Si-HAP and HAP are according to Eq. (1) and Eq. (2), respectively:



- $\beta\text{-Ca}_3(\text{PO}_4)_2$, powder providing the calcium and phosphorous, is prepared by heating the apatitic tricalcium phosphate ($\text{Ca}_9(\text{HPO}_4)(\text{PO}_4)_5(\text{OH})$: TCPa). Ca-deficient apatite powder was synthesized by rapid reaction between the calcium hydroxide and orthophosphoric acid according to the method described by Elouahli et al. [26]. Upon heating to 900°C , Ca-deficient apatite will transform to the reactive tricalcium phosphate ($\beta\text{-TCP}$) with the loss of water according to the following reaction (Eq. (3)):



- SiO_2 powder with amorphous structure is purchased from Alfa Aesar, (99.9%, Germany)
- CaCO_3 powder with a floury appearance is of quality Skora (99.9%, precipitated calcium carbonate).

Reactive powders were weighed and homogeneously mixed in form of paste with absolute ethanol using an agate mortar. The molar ratio Ca/P of HAP and Ca/(P+Si) of Si-HAP were equal to 1.67. The milled paste was then dried at 80°C for 24h to remove the ethanol. Following that, the dried mixture was crushed and heated to 1100°C at a rate of $5^\circ\text{C}/\text{min}$, and subsequently held at that temperature for 6 hours.

2.2. Characterization of powders

The identification of different crystal phases were determined by X-ray diffraction (BRUKER D8 ADVANCED. Copper $\text{K}\alpha$ radiation ($\lambda = 1.5406$) with 50kV and 20mA) and Fourier Transform Infrared spectroscopy (KBr pellet method, SHIMADZU FTIR-8400S). Structural characterization for the prepared samples was carried out with FullProf program (WinPLOTR 2017). Calculating the distortion of the PO_4 tetrahedrons can provide an estimation of the structure distortion. The tetrahedral distortion index was obtained from the calculated data using the relation (Eq. (4)):

$$D_{ind} = \frac{\sum_{i=1}^6 (\text{OPO}_i - \text{OPO}_m)^2}{6} \quad (4)$$

Where OPO_i denotes the six angles between P and the four O atoms of the phosphate tetrahedron and OPO_m is the average angle (around 109.17°).

Crystallinity of the powder was evaluated from XRD pattern using the following equation [27]:

$$X_c = 1 - \left(\frac{V_{112/300}}{I_{300}} \right) \quad (5)$$

Where X_c is the crystallinity degree, I_{300} is the intensity of (300) reflection and $V_{112/300}$ is the intensity of the hollow between (112) and (300) reflection. The density measurements were performed using a helium pycnometer (Accupyc 1330 Micromeritics).

2.3. Dissolution tests

The dissolution tests were carried out under acidic medium (similar to the process of acidification of the extracellular environment of osteoclasts) at pH close to 4.8 ± 0.2 involved by the in vivo degradation of the phosphocalcic implants [28]. The calcined powder was manually ground, and the particles less than $125 \mu\text{m}$ were separated by sieving. 200 mg of each sample was individually soaked in 100 ml of buffer solution of acetic acid-sodium acetate ($\text{pH} = 4.8 \pm 0.2$) at constant temperature of $37.0 \pm 0.1^\circ\text{C}$ for fixed periods of time. The solution was kept under mechanical agitation and at sufficient speed to keep all the grains in suspension. At the end of each period, the liquid phase was separated and analysed.

The ion concentrations of Ca^{2+} , PO_4^{3-} and SiO_4^{4-} were determined by Inductively Coupled Plasma-Atomic Emission Spectrometers (ICP-AES) (ThermoJarrel Ash. Atom Scan 16).

3. Results and discussion

3.1. Powder characterization

3.1.1. Structural study results

In Fig. 1 are shown the X-ray diffraction patterns for the HAP and Si-HAP powders. The result shows that the ceramics are composed of a single well-crystallized phase of apatite structure, which all peaks belong to the PDF file N° 9-432. There is no sign of presence of impurities such as CaO or (α or β)-Ca₃(PO₄)₂ or the precursor phases as SiO₂ or CaCO₃. The reaction between β -TCP, CaCO₃ and SiO₂ powders is total.

It is clear that the introduction of silicon had no significant influence on the overall profile of XRD patterns. However, it can be seen in the X-ray diagram Si-HAP (Fig.1) a slight lowering of crystallinity, visible in the slightly less defined peak (112) and a slight decreasing in the crystallinity degree has been found (Si-HAP ($X_c=0.91$) and HAP ($X_c=0.92$)).

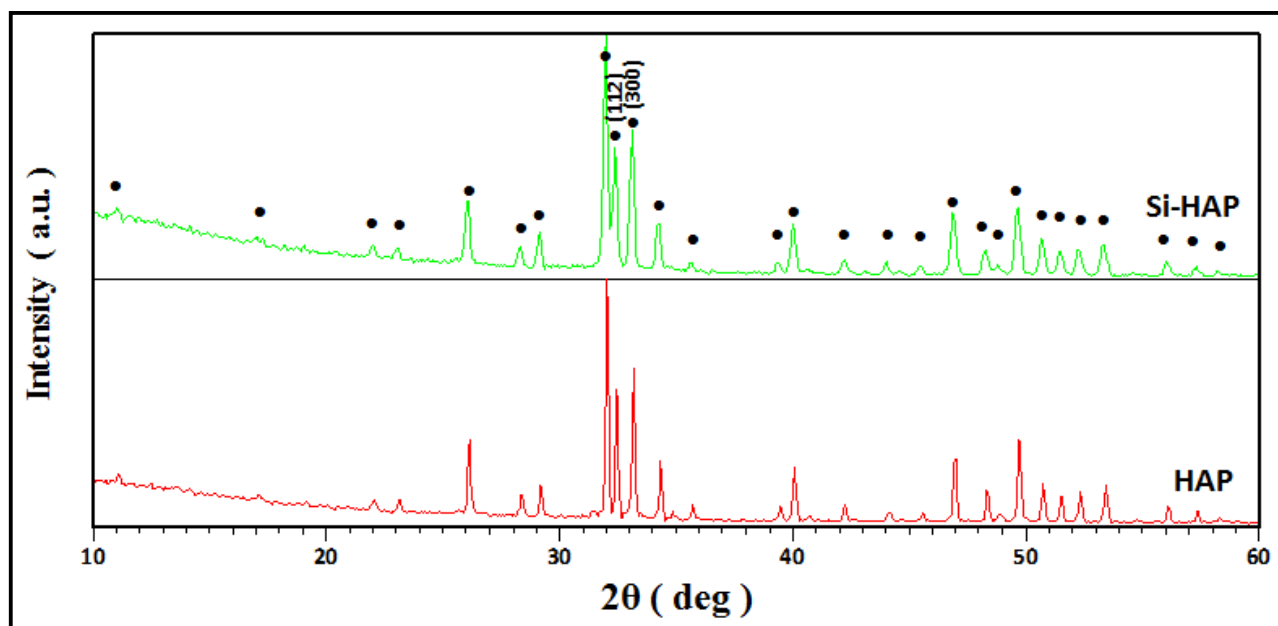


Figure 1: XRD patterns of prepared powders HAP and Si-HAP. (● HAP)

The lattice parameters and distortion of the hydroxyapatite phase are given in Table 1. The results show for unsubstituted hydroxyapatite a decrease of the lattice parameter (a-axis and c-axis) and of the cell volume compared to the theoretical HAP values. The calculated index value ($D_{ind} = 4.156 \text{ \AA}$) is higher than the theoretical value ($D_{ind} = 3.080 \text{ \AA}$).

The substitution of PO₄³⁻ by SiO₄⁴⁻ in the hydroxyapatite structure induces an increase of the lattice parameter (a-axis and c-axis) and of the cell volume compared to the unsubstituted HAP values. These results are in accordance with different previous studies [29-31]. The calculated index value ($D_{ind} = 4.682 \text{ \AA}$) is greater than the theoretical and the unsubstituted HAP value. Substitution of the PO₄³⁻ by the SiO₄⁴⁻ group leads to a distortion in the network.

Table 1: Structural refinement results: lattice parameters, unit cell volumes and tetrahedral distortion index (D_{ind}) of HAP.

| Sample | a (Å) | b (Å) | c (Å) | V(Å ³) | D_{ind} |
|----------------------|--------|--------|--------|--------------------|-----------|
| HAP _(the) | 9.4190 | 9.4190 | 6.8800 | 529.16 | 3.080 |
| HAP | 9.4072 | 9.4072 | 6.8731 | 526.7494 | 4.156 |
| Si-HAP | 9.4110 | 9.4110 | 6.8812 | 527.7963 | 4.682 |

3.1.2 FTIR analysis

Fig. 2 shows the FTIR spectra of the prepared samples HAP and Si-HAP. The bands at 3572 cm^{-1} and 633 cm^{-1} are characteristic of OH groups in the hydroxyapatite. The intense bands at 1045 cm^{-1} and 962 cm^{-1} corresponds to P-O stretching vibration modes, while the doublet at $603\text{-}569\text{ cm}^{-1}$ corresponds to bending O-P-O mode. In addition, the broad band at 3468 cm^{-1} was attributed to the moisture in the samples.

Besides the HAP bands, new bands appear at 891 cm^{-1} and 752 cm^{-1} assigned to the SiO_4 group [32]. No other compound, especially calcium silicate is evidenced on the X-ray diffraction pattern, and so these bands can be surely attributed to SiO_4 groups, in the apatite lattice.

The significant effect of the silicon addition was the decrease in the hydroxyl stretching bands at 3571 cm^{-1} and 631 cm^{-1} and phosphate stretching bands at 965 cm^{-1} . This can be related to the substitution of PO_4^{3-} by SiO_4^{4-} tetrahedrons, within the hydroxyapatite structure.

The incorporation of silicon ion in the hydroxyapatite phase induces a reduction of the amount of hydroxyl groups to compensate for the extra negative charge of the silicates group. The proposed mechanism to explain these structural changes is the following:

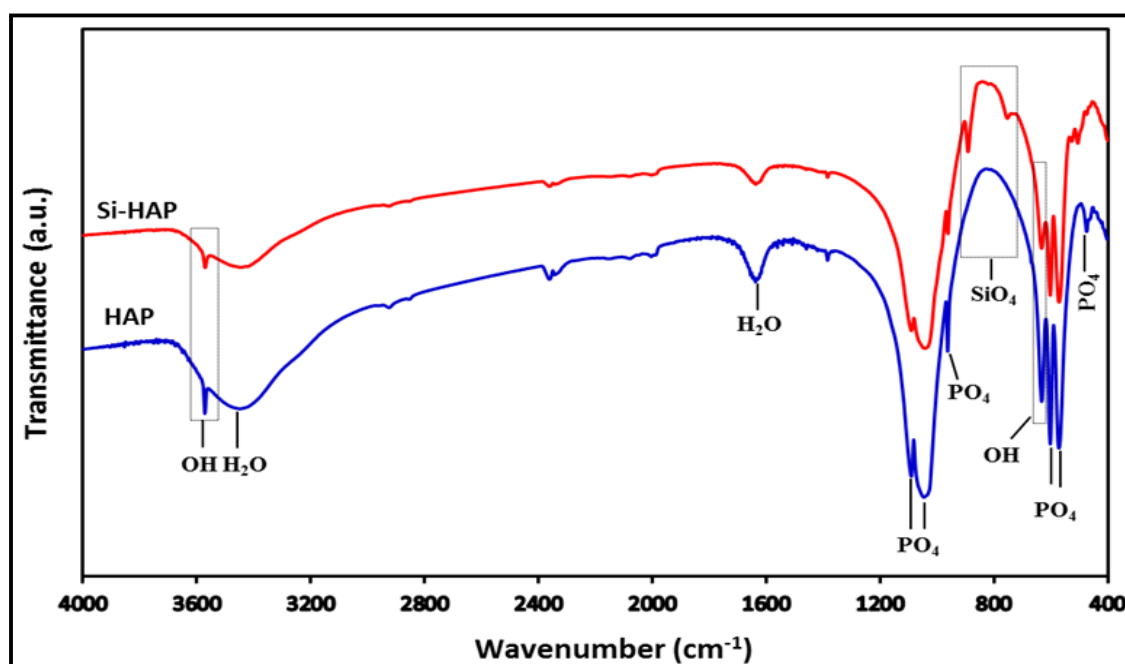
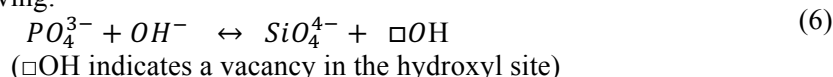


Figure 2: FT-IR spectra of prepared powders HAP and Si-HAP

3.3. Dissolution tests

Fig. 3 shows the results of Calcium, Phosphor and Silicone ions concentrations with the immersion time of two samples (Si-HAP and HAP). The concentration of Calcium and Phosphor released by Si-HAP, increase with the immersion time. However, the ion concentrations released by HAP, remain unchanged after 1h of immersion. Fig.3(c) shows the rapid release of the silicon ions from the beginning of the immersion.

This results show that dissolution of Si-HAP is higher compared to unsubstituted HAP; it's in agreement with previous studies [8,16, 21, 33, 34]. A.E. Porter and al. [16] observed that the dissolution of the substituted silicon ceramic increases with silicon increase. Dissolution was observed to follow the order $1.5\text{wt}\% \text{ Si-HA} > 0.8\text{wt}\% \text{ Si-HA} > \text{pure HA}$, suggesting that silicate ions increase the solubility of HAP [16]. Yu and al. [33] found that the dissolution was observed to follow the order $\text{Si-HA}1.6 > \text{Si-HA}0.8 > \text{HA}$, suggesting that the silicate increased the solubility. Some authors have described that the fast dissolution of Si-hydroxyapatite is due to the migration to the positioning of whether the grain boundary [13], and a smaller grain size with more triple-junctions per unit area, facilitating increased dissolution at the surface [16,34]. In general, the research works agreed that at 1200°C the grain size of Si-HAP decreases with increasing Si content and the density slightly increases with increasing heat-treatment temperatures. The results of our work show that at 1100°C , the effect of Si on the density of Si-HAP samples is less significant. The density of Si-HAP samples is close to that of

HAP sample successively equal to 2.90g/cm^3 and 3.02g/cm^3 . We showed that the substitution of PO_4^{3-} by SiO_4^{4-} groups leads to the hydroxyapatite lattice distortion. This structural change could decrease the stability of the hydroxyapatite structure and increase the solubility. The composition and the structure of the monophasic bioceramics, prepared in this work by simple solid-state reaction, appear very promising for biological applications.

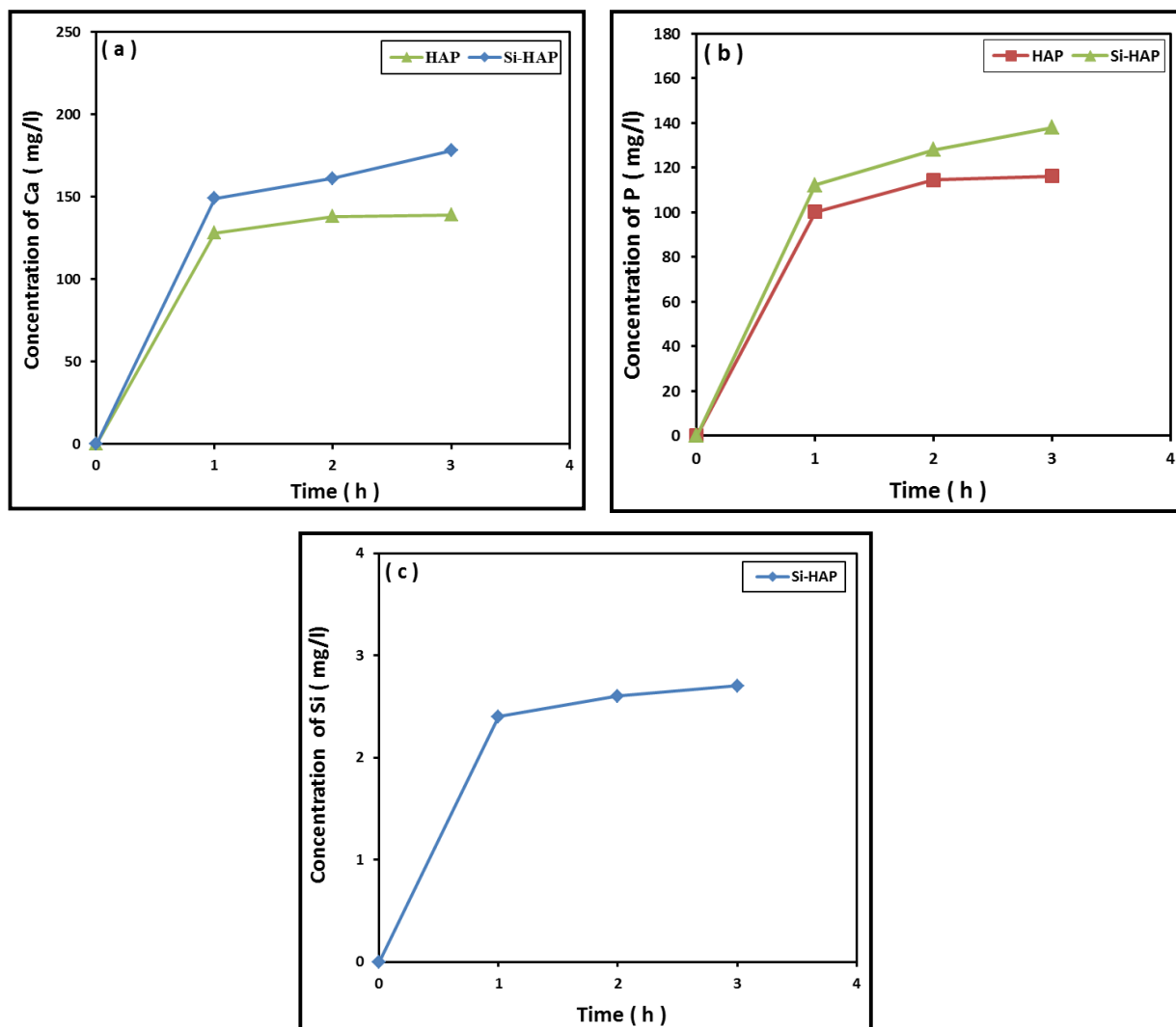


Figure 3: Variation of concentration with immersion time of: (a) calcium, (b) phosphor and (c) silicon ions.

Conclusion

Silicon substituted hydroxyapatite Si-HAP and pure HAP bioceramics were prepared by simple solid-state reaction at 1100°C for 6 hours of intimate mixtures of reactive calcium phosphate compounds with or without silicon dioxide. The results show the formation of monophasic Si-HAP and HAP bioceramics. The incorporation of silicon ions in the hydroxyapatite lattice distorts its structure and promotes the dissolution. The Si-HAP bioceramics could be more bioactive material compared to the pure HAP.

References

1. Z. Sheikh, S. Najeeb, Z. Khurshid, V. Verma, H. Rashid, M. Glogauer, *Materials*. 8(9) (2015) 5744–5794.
2. B. Zhao, H. Hu, S.K. Mandal, R.C. Haddon, *Chem. Mater*, 17 (2005) 3235–3241.
3. M.B. Conz, J.M. Granjeiro, G. d.A. Soares, *J. Appl. Oral. Sci.* 19 (4) (2011) 337–342
4. M. Mastrogiacoma, A. Muraglia, V. Komlev, F. Peryin, F. Rustichelli, A. Crovace, R. Cancedda, *Orthod. Craniofacial. Res.* 8 (2005) 277–284.

5. JC. Elliott, *Stud Org Chem.* 18 (1994) 63–103.
6. RZ. LeGeros, *Monogr Oral Sci.* 15 (1990) 1–201.
7. A.M. Pietak, J.W. Reid, M.J. Stott, M. Sayer, *Biomaterials* 28 (2007) 4023–4032.
8. S.R. Kim, J.H. Lee, Y.T. Kim, D.H. Riu, S.J. Jung, Y.J. Lee, S.C. Chung, Y.H. Kim, *Biomaterials.* 23 (2003) 1389–1398.
9. E. M. Carlisle, *Science.* 167(1970) 179.
10. E. M. Carlisle, *Calc. Tissue Int.* 33(1981) 27.
11. Y. Belmamouni, M. Bricha, J. Ferreira, K. El Mabrouk, *Int. J. Appl. Ceram. Technol.* 12 (2) (2015) 329–340.
12. N. Patel, R. A. Brooks, M. T. Clarke, P. M. T. Lee, N. Rushton, I. R. Gibson, S. M. Best, W. Bonfield, *J. of Material Science.* 16 (2005) 429–440.
13. A. E. Porter, C. M. Botelho, M. A. Lopes, JD. Santos, SM. Best, W. Bonfield. *J Biomed Mater Res.* 69A (2004) 670–679.
14. K. Szurkowska, J. Kolmas, *Progress in Natural Science: Materials International* 27 (2017) 401–409
15. M. Honda, K. Kikushima, Y. Kawanobe, T. Konishi, M. Mizumoto, M. Aizawa, *J. Mater. Sci. Mater. Med.* 23 (2012) 2923–2932.
16. A.E. Porter, N. Patel, J.N. Skepper, S.M. Best, W. Bonfield, *Biomaterials* 24 (2003) 4609–4620
17. P. A. Sindu, E. Kolanthai, R. V. Suganthi, K. T. Arul, E. Manikandan, L. H. Catalani, S. N. Kalkura, *Journal of Photochemistry & Photobiology, B: Biology* 175 (2017) 163–172.
18. A. M. Pietak, J. W. Reid, M. J. Stott, M. Sayer, *Biomaterials* 28 (2007) 4023–4032
19. C. M. Botelho, R. A. Brooks, G. Spence, I. McFarlane, M. A. Lopes, S. M. Best, J. D. Santos, N. Rushton, W. Bonfield, *J Biomed Mater Res.* 78A (2006) 709–20.
20. M. S. Shojai, M. T. Khorasani, E. D. Khoshdargi, A. Jamshidi, *Acta Biomaterialia* 9 (2013) 7591–7621
21. L. T. Bang, S. Ramesh, J. Purbolaksono, Y. C. Ching, B. D. Long, Hari Chandran, S. Ramesh, R. Othman, *Materials and Design* 87 (2015) 788–796.
22. X. L. Tang, X. F. Xiao, R. F. Liu, *Mater. Lett.* 59 (2005) 3841–3846.
23. N. Zhang, D. Zhai, L. Chen, Z. Zou, K. Lin, J. Chang, *Materials Science and Engineering C* 37 (2014) 286–291.
24. M. Vallet-Regi, D. Arcos, *J. Mater. Chem.* 15 (15) (2005) 1509.
25. R. Borşa, M. Freche, G. Coşmeleaţă, J. Lacout, S. Ciuca. *U.P.B. Sci. Bull.* 70B (2008) 3.
26. A. Elouahli, E. Gourri, B. El ouatli, M. Jamil, H. Khallok, Z. Hatim. *IJSER.* 7(2016) 764–769.
27. E. Landi, A. Tampieri, G. Celotti, S. Sprio, J. Eur. Ceram. Soc. 20 (2000) 2377–2387.
28. P. Frayssinet, N. Rouquet, T. Tourenne, J. Fages, D. Hardy, G. Bonel. *Cells and Materials.* 3(4) (1993) 383–94.
29. S. Gomes, G. Renaudin, A. Mesbah, E. Jallot, C. Bonhomme, F. Babonneau, J.-M. Nedele, *Acta Biomaterialia* 6 (2010) 3264–3274.
30. T. Tian, D. Jiang, J. Zhang, Q. Lin, *Materials Science and Engineering C* 28(2008) 57–63.
31. M. Palard, *Thesis of Limoges University*, N°: 2007-XX. (2007)
32. T. Leventouri, C. E. Bunaciu, V. Perdikatsis, *Biomaterials* 24 (2003) 4205–4211.
33. H. Yu, K. Liu, F. Zhang, W. Wei, C. Chen, Q. Huang, *Silicon* (2015) 1–11.
34. A. E. Porter, *Micron* 37 (2006) 681–688.

(2018) ; <http://www.jmaterenvirosci.com>